

Demonstration of a Quantum Controlled-NOT Gate in the Telecom Band

Jun Chen,¹ Joseph B. Altepeter,¹ Milja Medic,^{1,2} Kim Fook Lee,¹ Burc Gokden,¹ Robert H. Hadfield,³ Sae Woo Nam,³ and Prem Kumar^{1,2}

¹Center for Photonic Communication and Computing, EECS Department
Northwestern University, 2145 Sheridan Road, Evanston, IL 60208-3118

²Department of Physics and Astronomy, Northwestern University, 2145 Sheridan Road, Evanston, IL 60208-3118

³National Institute of Standard and Technology, 325 Broadway, Boulder, CO 80305

We present the first quantum controlled-NOT (CNOT) gate realized using a fiber-based indistinguishable photon-pair source in the 1.55 μm telecommunications band. Using this free-space CNOT gate, all four Bell states are produced and fully characterized by performing quantum state tomography, demonstrating the gate's unambiguous entangling capability and high fidelity. Telecom-band operation makes this CNOT gate particularly suitable for quantum information processing tasks that are at the interface of quantum communication and linear optical quantum computing.

PACS numbers: 42.50.Dv, 03.67.Hk, 03.67.Lx, 42.65.Lm

Photons in the telecommunications band (e.g., 1.55 μm wavelength) are ideally suited for carrying quantum information over a large-scale quantum network, because such a network could use low-loss optical fibers. Moreover, photons in optical fibers interact weakly with their surrounding environments, displaying low decoherence. These desirable features, together with easily realizable single qubit operations, make the telecom-band photons a prominent candidate for various quantum-information-processing applications [1]. The main obstacle to using photons for quantum computing tasks—including the most basic quantum computing operation, the controlled-NOT (CNOT) gate—is the miniscule interaction between two photonic ‘qubits’ (quantum bits). Fortunately, this obstacle has been circumvented by the arrival of a seminal paper [2] in which the required nonlinearity between photons has been effectively transferred to measurement and post-selection.

This Letter describes efforts to apply this new quantum computational paradigm to the fundamental CNOT operation using telecom-band photons. Previous implementations of the CNOT gate (or a similar controlled-phase gate) [3, 4, 5, 6, 7, 8, 9] utilized photons from spontaneous parametric down-conversion (SPDC) in second-order ($\chi^{(2)}$) nonlinear crystals. Those SPDC photons are not telecom band, and are therefore subject to much higher losses when transferred through optical fiber. Although telecom-band photons can also be generated via the SPDC process, these photons are naturally emitted into a large number of spatial and spectral modes, resulting in significant losses when coupled to a single-mode optical fiber. The usage of SPDC photon sources in fiber quantum networks is thus limited. However, recently developed fiber-based sources [10, 12] intrinsically avoid this issue. In this Letter we demonstrate, for the first time to the best of our knowledge, a quantum CNOT gate at a telecom-band wavelength. This gate uses three separate yet individually crucial experimental components: a fiber-based indistinguishable photon-pair source [10], the

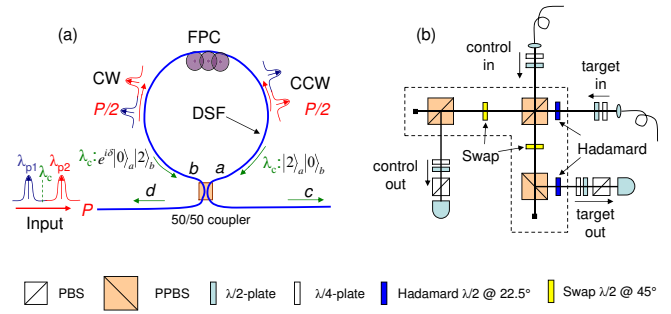


FIG. 1: (color online) Key components of the CNOT gate. (a) Quantum splitter (QS) source. Two identical photon-pair wavefunctions interfere at a 50/50 beam splitter with zero phase difference, resulting in deterministic splitting of the photon pair. DSF, dispersion-shifted fiber; FPC, fiber polarization controller; CW, clockwise; CCW, counterclockwise. (b) Structure of the quantum CNOT gate. (P)PBS, (partially) polarizing beam splitter.

free-space linear optical components of the CNOT gate itself, and a heralding detection system composed of one superconducting single-photon detector (SSPD) and one InGaAs/InP avalanche photodiode (APD).

Indistinguishable (or *identical*) photons refer to photons having the same spatial, temporal (frequency) and polarization mode structure, and constitute a critical resource for linear optical quantum computing. Quantum interference arising from the bosonic nature of indistinguishable photons, such as the well-known Hong-Ou-Mandel (HOM) interference [11], lies at the heart of linear optical quantum computing. Our group has recently demonstrated a HOM dip of approximately 94% visibility (without any accidental subtraction) using a fiber-based indistinguishable photon-pair source [10], which we dubbed a “quantum splitter”, or QS for short. The QS source is shown in Fig. 1 (a), and can be conveniently summarized in terms of “time-reversed Hong-Ou-Mandel interference”. To see how, consider a dual-frequency pump [12], which consists of two copolarized, temporally overlapped, and spectrally distinct (center wave-

lengths λ_{p1} and λ_{p2}) pulses with equal power, entering a fiber Sagnac loop from port d . The Sagnac loop is composed of a 50/50 fiber coupler, a piece of dispersion-shifted fiber (DSF), and a fiber polarization controller (FPC). The total peak pump power P is equally split into two dual-frequency, counter-propagating pump pulses of power $P/2$. The DSF inside the Sagnac loop is chosen such that its zero-dispersion wavelength (λ_0) is close to the mean wavelength (λ_c) of the pump's two central wavelengths [i.e., $\lambda_0 \simeq \lambda_c \equiv 2\lambda_{p1}\lambda_{p2}/(\lambda_{p1} + \lambda_{p2})$] to maximize the four-wave mixing (FWM) scattering efficiency [13]. The FWM process of interest is of the reverse degenerate type [12, 14], wherein two pump photons of different frequencies (ω_{p1} and ω_{p2}) annihilate to produce a pair of energy-degenerate daughter photons at their mean frequency (ω_c), satisfying $\omega_{p1} + \omega_{p2} = 2\omega_c$. When their powers are balanced, the clockwise pump and the counterclockwise pump scatter copolarized FWM photon-pairs with equal probability. The two probability amplitudes are then made to interfere at the 50/50 fiber coupler; their phase difference δ is controlled by the setting of the intraloop FPC. For an input state $|\Psi\rangle_{\text{in}} = (|2\rangle_a|0\rangle_b + e^{i\delta}|0\rangle_a|2\rangle_b)/\sqrt{2}$, the output state for a standard symmetric beam splitter is given by $|\Psi\rangle_{\text{out}} = (1 - e^{i\delta})\Psi_{2002}/2 + i(1 + e^{i\delta})\Psi_{11}/2$, where $\Psi_{2002} \equiv (|2\rangle_d|0\rangle_c - |0\rangle_d|2\rangle_c)/\sqrt{2}$ and $\Psi_{11} \equiv |1\rangle_c|1\rangle_d$. It is transparent from the above expressions that if we set δ to be 0, we will perform the reverse operation ($\Psi_{2002} \Rightarrow \Psi_{11}$) of the conventional HOM interference ($\Psi_{11} \Rightarrow \Psi_{2002}$) with $\Psi_{2002} \equiv (|2\rangle_a|0\rangle_b + |0\rangle_a|2\rangle_b)/\sqrt{2}$, and hence the interpretation as ‘‘time-reversed HOM interference’’. The name ‘‘quantum splitter’’, however, stems from the intended use of such a device to *deterministically* split two identical photons. Note that in this QS setting, the Sagnac loop also splits the classical pump into two equal-powered components in ports c and d .

The output of the QS source is fed into a CNOT gate based on three partially polarizing beam splitters (PPBS), as shown in Fig. 1 (b). Requiring only two input photons (control and target) with no ancillary photons, this simple CNOT gate is probabilistic in nature [5, 6, 7]; however it is still in principle scalable when coupled with linear optical quantum non-demolition measurements [4]. The PPBSs adopted in the CNOT gate design are optical devices which completely reflect vertically-polarized light (V), and have a reflectivity of 1/3 for horizontally-polarized light (H). Non-classical interference of the HOM type happens only at the central PPBS, and only for horizontally-polarized input qubits (HH , where the first H refers to the control qubit and the second H refers to the target qubit). The other two PPBSs, each preceded by a swap gate (a half-wave plate with its principle axis set to 45° , performing $H \leftrightarrow V$), exist to equalize the probability amplitudes for all other inputs (VV , VH and HV). With the logic-basis definitions $0 \equiv V$ and $1 \equiv H$, it is a simple exercise to show that the gate

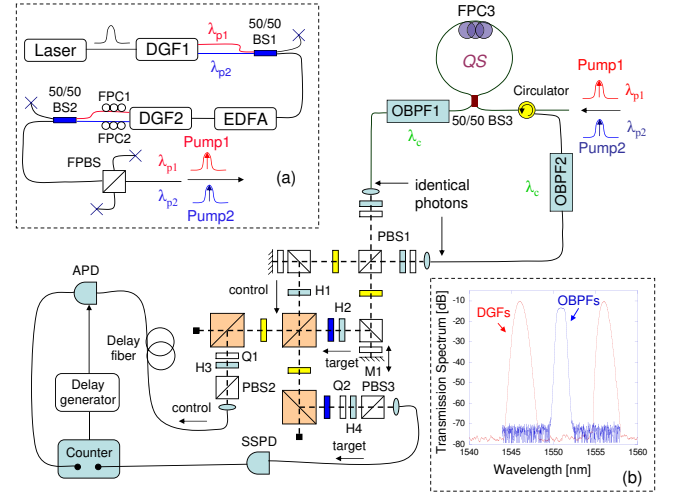


FIG. 2: (color online) Schematic experimental setup. Identical photons generated by the QS source serve as input control and target qubits to the CNOT gate, whose output is collected using a heralding detection scheme with a superconducting single-photon detector (SSPD) and an avalanche photodiode (APD). BS, beam splitter; OBPF, optical bandpass filter. Inset (a): Preparation of the dual-frequency copolarized pump. DGF, double-grating filter; FPBS, fiber polarizing beam splitter; EDFA, erbium-doped fiber amplifier. Inset (b): Transmission spectra of the OBPFs and DGFs.

succeeds with a probability of 1/9 in performing the following CNOT transformation: $\alpha|VV\rangle + \beta|VH\rangle + \gamma|HV\rangle + \delta|HH\rangle \rightarrow \alpha|VV\rangle + \beta|VH\rangle + \gamma|HH\rangle + \delta|HV\rangle$, conditioned on the detection of one and only one photon in each of the output modes.

Figure 2 depicts the experimental setup for demonstrating the CNOT gate’s operation. We pump the QS source with a dual-frequency copolarized pump, which is obtained from spectral carving of a broadband mode-locked femtosecond laser (repetition rate $\simeq 50$ MHz). The details of the dual-frequency pump have been described in Ref. [12], and is shown in inset (a) for completeness. To recapitulate, we select our two pump central wavelengths ($\lambda_{p1} = 1545.95$ nm and $\lambda_{p2} = 1555.92$ nm, pulse width $\simeq 5$ ps) by passing the broad laser spectrum through two double-grating filters [DGF1 and DGF2, FWHM $\simeq 0.8$ nm for each passband; see inset (b) in Fig. 2 for their spectral shape]. An erbium-doped fiber amplifier is sandwiched in between the two DGFs to provide pump power variability. Each pump pulse’s timing, polarization, and power can be individually controlled, so that at the output of the fiber polarizing beam splitter we obtain copolarized, equal-powered, dual-frequency pump pulses with overlapped timing. We then direct this pump toward the QS source. A circulator is placed before the Sagnac loop, which redirects the Sagnac-reflected photons to a separate spatial mode. A pair of optical bandpass filters (OBPF1 and OBPF2) with identical transmission spectrum [center wavelength $\lambda_c = 1550.92$ nm, pass-band FWHM $\simeq 0.8$ nm, see inset (b) of Fig. 2] are uti-

lized at the output ports of the Sagnac loop to select the spatially separated identical photons at λ_c . The OBPFs also provide the necessary > 100 dB isolation from the pump in order to effectively detect those filtered photons. Before pumping with the dual-frequency pump, the 300 m-long DSF in the Sagnac loop is immersed in liquid nitrogen to suppress spontaneous Raman scattering [15, 16], and we ensure that thermal equilibrium is reached between the DSF and its liquid-nitrogen environment. We then align the Sagnac loop to its QS setting by using a continuous-wave tunable laser set at wavelength λ_c as the input, and adjusting FPC3 so that the output powers from OBPF1 and OBPF2 are proportional to each filter’s individual transmission efficiency [10].

Coming out of the QS source, the two identical photons are collimated into free space, and directed through several optical elements. The goal of these optics is to precisely control the timing and polarization of each photon, so that they are maximally overlapped when they interfere nonclassically at the central PPBS of the CNOT gate. A translation stage is placed under the mirror M1 to precisely match the paths of the two photons. The first polarizing beam splitter (PBS1) then separates the two photons into separate paths. The other two PBSs, each with a 45°-quarter-wave plate and a mirror behind, function just like two perfectly reflecting mirrors. This configuration ensures that translating M1 does not cause misalignment of the input target photon. The control and target photons enter the CNOT gate with well-defined polarization (vertical) and timing (within their $\simeq 5$ ps pulse duration). Half-wave plates H1 and H2 are used to define the logical values of input qubits, while two polarization analyzers (Q1/H3/PBS2 and Q2/H4/PBS3) are employed at the output to examine the polarization of the output qubits.

One of the primary obstacles to the implementation of telecom-band quantum information protocols is the lack of good single-photon detectors, in contrast to the high quality single-photon detectors available for visible wavelengths. For this experiment, we had access to both cryogenically cooled SSPDs and InGaAs APDs. The SSPDs [18, 19] have low efficiency ($\simeq 1\%$) and low dark-count probability ($\simeq 3 \times 10^{-6}$ counts/gate). The APDs (Epitaxx, EPM 239BA) have higher efficiency ($\simeq 20\%$) and much higher dark-count probability ($\simeq 3 \times 10^{-3}$ counts/gate). (These rates should be compared with the inferred FWM production rate in this experiment— $\simeq 0.15$ FWM photon pairs/gate and 0.15^2 multiple-photon pairs/gate.) In order to maximize the joint efficiency while minimizing dark counts, a heralded detection scheme [17] was implemented where one higher efficiency APD is triggered by one low dark-count-rate SSPD. In this way the APD has far fewer opportunities to generate dark counts, while still allowing us to benefit from its higher quantum efficiency.

The NbN-meander SSPD that we employed in the ex-

periment is a nanoscale superconducting wire operated at a temperature of $\simeq 3$ K and biased close to its critical current. When a photon strikes the wire, it forms a hot spot which momentarily breaks the superconductivity and causes a transient voltage on the device that is registered as a photon detection. The entire process happens very quickly, leading to a dead time of $\simeq 10$ ns. In order to use this signal detector as a herald of the idler photon, we need to delay the idler photon in a “delay fiber” to allow an electronic heralding trigger pulse to arrive at the APD. At the same time an electrical pulse is delayed (using a Stanford Research Systems DG535) and sent to a photon coincidence counter. The triggered APD output is reshaped by a field-programmable-gate-array board (not shown in Fig. 2) and sent back to the same photon counter to be recorded as a coincidence count. We scan the delay time τ given by the delay generator to locate the “coincidence peak” (corresponding to $\tau = \tau_0$), where the count value is significantly higher than its neighboring peaks, which indicates that each member of the photon pair from the same optical pulse has been captured by the SSPD/APD combination. This coincidence peak value is hereafter referred to as (total) coincidences. Accidental coincidences, mainly due to Raman noise and dark counts, are conveniently recorded by setting $\tau = \tau_0 - 20$ ns, where 20 ns is the period between consecutive pump pulses.

To characterize the performance of our CNOT gate, we first input four possible logical basis states for the control (C) and target (T) qubits: $|V\rangle_C|V\rangle_T$, $|V\rangle_C|H\rangle_T$, $|H\rangle_C|V\rangle_T$, $|H\rangle_C|H\rangle_T$, and record coincidences and accidental coincidences for each output state in the above logical basis. We then subtract the latter coincidences from the former to get true coincidences for each case, which, after being transformed into probabilities, are plotted in Fig. 3 (a), displaying the truth table for the gate. It can be seen from Fig. 3 (a) that the gate works quite well in the logical basis, with an average fidelity (probability of getting the correct output averaged over all logical inputs) of 0.87 (87%). During the experiment, we apply a triangular-wave voltage to a piezoelectric transducer (not shown in Fig. 2) placed within the translation stage under M1; this dithering technique [21] effectively averages out single-photon interference originating from the QS source due to the experiment’s high pump power and stabilizes the single-count measurements recorded by the SSPD. Such a technique is not necessary in the low pump-power regime, as single stray photons become negligible.

As a demonstration of the entangling capability of the gate, we send in four separable states $|D\rangle_C|V\rangle_T$, $|A\rangle_C|V\rangle_T$, $|D\rangle_C|H\rangle_T$, and $|A\rangle_C|H\rangle_T$ ($|D\rangle \equiv |H\rangle + |V\rangle$ and $|A\rangle \equiv |H\rangle - |V\rangle$), which theoretically should be transformed by the gate into four maximally entangled Bell states: $|\Phi^\pm\rangle$, $|\Psi^\pm\rangle$, respectively. We then characterize each output state using quantum-state tomography, and reconstruct its density matrix using the maximum like-

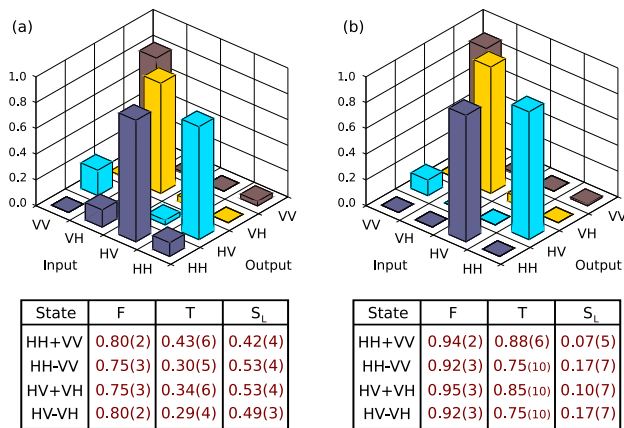


FIG. 3: (color online) (a) Experimentally measured truth table for the CNOT gate in the logical basis (data represent coincidence counts minus accidental counts due to Raman noise and detector dark counts). The highest peak values are: 0.81 ± 0.05 (VV, VV), 0.85 ± 0.06 (VH, VH), 0.94 ± 0.07 (HV, HH), and 0.88 ± 0.06 (HH, HV). Also shown is the Bell-state characterization for the same gate. Fidelity (F), tangle ($T \equiv \text{Concurrence}^2$), and linear entropy ($S_L \equiv \frac{4}{3} \{1 - \text{Tr}(\rho^2)\}$) are given for all CNOT-generated Bell states. (b) The same truth table and Bell-state data is shown after subtracting accidental coincidences due to multiple photon-pair production. Peak values are: 0.88 ± 0.05 , 0.98 ± 0.06 , 0.94 ± 0.05 , and 0.99 ± 0.05 .

likelihood method [22, 23]. Corrections are made on the final results to account for small pump-power fluctuations during the measurements. The reconstructed density matrix $\hat{\rho}$ for each output state is then used to calculate its fidelity with its theoretically predicted Bell state (e.g., $F_{\Psi^-} \equiv \langle \Psi^- | \hat{\rho} | \Psi^- \rangle$), its tangle [1], and its linear entropy [1, 22, 24]. The results are summarized in Fig. 3 (a).

While mode mismatch explains some of the deviation from ideal CNOT performance shown in Fig. 3 (a), the mode matching quality implied by the source's HOM visibility [10] only accounts for a degradation of entangled fidelities to $\simeq 95\%$. Imperfect optics account for $\simeq 1\%$ of additional error. The major source of error is, in fact, due to multiple-pair creations in the identical-photon source. In comparison with Ref. [10], here we pump the system with relatively high pump power (total average power $P = 450 \mu\text{W}$) to combat the gate's inherent 8/9 loss. This pump power leads to $\simeq 15\%$ of all gate inputs arising from multiple-pair events. In order to accurately characterize the performance of the CNOT gate on *single* pairs of input photons, we estimate the multiple-pair contributions to the measurements, subtract them from the data, and show the resulting CNOT gate performance in Fig. 3 (b). These much higher fidelities and gate performance ($\simeq 95\%$ canonical-basis fidelity and $\simeq 93\%$ entangled fidelities) are consistent with our previous error estimates.

To estimate the multiple-pair contributions to the data, we perform a new type of maximum-likelihood process tomography [25]. By assuming that only linear optics are present within our gate, we model a process as

the transformations of each of four single-photon input modes (two polarizations and two spatial modes) into six single-photon output modes (the input modes plus the two PPBS dump ports). These four transformations can then be used to predict the gate's output for any input. Note that in order to minimize the search parameters, we only conduct the search over processes that do not cause decoherence, and thus the search is *not* a complete process tomography. However, we are confident that the resulting "pure" process can be used to estimate accidental coincidences from multiple pairs since it predicts with high precision all of our measured data (the average difference of the predicted and measured data was only 1.0 standard deviations, and the process fidelity between the predicted process and the ideal CNOT gate was $\simeq 95\%$).

In conclusion, we have demonstrated a telecom-band quantum CNOT gate and characterized it using a heralding scheme based on a superconducting single-photon detector. The authors would like to acknowledge support by the NSF under Grant No. EMT- 0523975.

-
- [1] M. A. Nielsen and I. L. Chuang, *Quantum Computation and Quantum Information* (Cambridge University Press, Cambridge, 2000).
 - [2] E. Knill, R. Laflamme, and G. J. Milburn, *Nature* **409**, 46-52 (2001).
 - [3] T. B. Pittman, M. J. Fitch, B. C. Jacobs, and J. D. Franson, *Phys. Rev. A* **68**, 032316 (2003).
 - [4] J. L. O'Brien *et al.*, *Nature* **426**, 264-267 (2003).
 - [5] N. K. Langford *et al.*, *Phys. Rev. Lett.* **95**, 210504 (2005).
 - [6] N. Kiesel *et al.*, *Phys. Rev. Lett.* **95**, 210505 (2005).
 - [7] R. Okamoto *et al.*, *Phys. Rev. Lett.* **95**, 210506 (2005).
 - [8] P. Walther and A. Zeilinger, *Phys. Rev. A* **72**, 010302(R) (2005).
 - [9] Z. Zhao *et al.*, *Phys. Rev. Lett.* **94**, 030501 (2005).
 - [10] J. Chen, K. F. Lee, and P. Kumar, *Phys. Rev. A* **76**, 031804(R) (2007).
 - [11] C. K. Hong, Z. Y. Ou, and L. Mandel, *Phys. Rev. Lett.* **59**, 2044-2046 (1987).
 - [12] J. Chen *et al.*, *Opt. Lett.* **31**, 2798 (2006).
 - [13] G. P. Agrawal, *Nonlinear Fiber Optics*, chapter 10 (Academic Press, San Diego, 2001).
 - [14] J. Fan, A. Dogariu, and L. J. Wang, *Opt. Lett.* **30**, 1530 (2005).
 - [15] H. Takesue, and K. Inoue, *Opt. Express* **13**, 7832 (2005).
 - [16] K. F. Lee *et al.*, *Opt. Lett.* **31**, 1905 (2006).
 - [17] M. A. Jaspan *et al.*, *App. Phys. Lett.* **89**, 031112 (2006).
 - [18] R. H. Hadfield *et al.*, *Opt. Express* **13**, 10846 (2005).
 - [19] C. Liang *et al.*, *Opt. Express* **15**, 1322 (2007).
 - [20] G. N. Gol'tsman *et al.*, *Appl. Phys. Lett.* **79**, 705 (2001).
 - [21] Y. J. Lu, R. L. Campbell, and Z. Y. Ou, *Phys. Rev. Lett.* **91**, 163602 (2003).
 - [22] D. F. V. James *et al.*, *Phys. Rev. A* **64**, 052312 (2001).
 - [23] J. B. Altepeter, E. R. Jeffrey, and P. G. Kwiat, *Advances in AMO Physics*, volume **52**, chapter 3 (Elsevier 2005).
 - [24] W. J. Munro, K. Nemoto, and A. G. White, *J. Mod. Opt.* **48**, 1239 (2001).
 - [25] J. L. O'Brien *et al.*, *Phys. Rev. Lett.* **93**, 080502 (2004).